Cryogenic Processing of Materials for Enhanced Product Life, Performance and Sustainability

I.S. Jawahir[1 *], Z. Pu[1], S. Yang[1], G. Rotella[1,2], Y. Kaynak[1], T. Lu[1]
A. Deshpande[1], D. Umbrello[1,3], O.W. Dillon Jr.[1]

[1]*Institute for Sustainable Manufacturing (ISM), University of Kentucky, Lexington, Kentucky, 40506, USA*
[2]*Dept. of Management and Production Engineering, Politecnico di Torino, Torino (TO), 10129, Italy*
[3]*Dept. of Mechanical, Energy and Management Engineering, University of Calabria, Rende (CS), 87036, Italy*

In recent years, the use of basic principles of sustainability science and engineering in new product development has been an emerging trend in manufacturing. Designing sustainable products and developing sustainable manufacturing processes have been a major research focus in sustainable manufacturing. This paper summarizes recent advances in manufacturing techniques involving novel cryogenic processing (machining and burnishing processes) of a range of aerospace, automotive and biomedical alloys (*AA 7075-T651, Inconel 718*, *Ni-Ti*, *AZ31B Mg*, *AISI 52100* and *Co-Cr-Mo* alloys) for achieving enhanced product performance, life and sustainability. This extensive study covers an analysis of surface integrity involving severe plastic deformation (*SPD*) induced by cryogenic processes in the materials, and the resulting performance enhancement through controllable ultrafine/nano grain structures, associated with significantly improved wear and corrosion resistance properties, and the generation of compressive residual stresses leading to improved fatigue life, along with more favorable phase transformation in these cryogenically processed materials. Encouraging results are obtained showing enormous potential for industry applications.

Keywords: cryogenic machining/burnishing, nano/ultrafine grains, surface integrity

1. INTRODUCTION

Machining is a functionally and economically advantageous severe plastic deformation (*SPD*) process, which involves large shear strains (typically 2–10) and highly localized strain-rates (up to 10^6 per second). Grain refinement occurs during machining due to dynamic recrystallization (*DRX*). Swaminathan et al. [1] show a significant grain refinement in the machined chip from machining of copper. The grain size was reduced to about 218 nm from over 20 μm. Further evidence was subsequently reported by Saldana et al. [2] showing the similarity between the microstructure in the chip and on the machined surface. The "white layer" formed on *AISI 52100* steel was shown to consist of nanocrystalline grains about 5-20 nm [3]. Sasahara [4] showed the correlation between the residual stresses on the machined surface and the fatigue life of the machined components.

Burnishing, an effective and *SPD* process, was studied by several researchers, some of whom also demonstrated burnishing-induced grain refinement. Zhang and Lindemann [5] created nanocrystalline surface layers in *AZ80* alloys by roller burnishing; the nano-scale grain structure was reported to improve the fatigue life of this material. Nikitin et al. [6] studied deep-rolled austenitic stainless steel *AISI 304* and *Ti6Al4V* alloys and their results show that nanocrystalline grain structure induced by deep-rolling was stable during short time annealing and that the isothermal fatigue in the low-cycle fatigue regime at high stress amplitudes does not alter the nanocrystalline surface layer up to 600 ℃.

Burnishing induces compressive residual stresses in the surface region. Zhang and Lindemann [5] show that roller burnishing improved the high-cycle fatigue strength of *AZ80* alloy by about 110%. Majzoobia et al. [7] also found that

much higher compressive residual stresses were generated on the surface in burnishing of several materials.

The temperatures generated during the *SPD* processes play a critical role on the grain size during and after *DRX*. Nano/ultrafine grains will grow at high temperatures. Since heating is often required for *ECAP*, the minimum grain size achieved is normally larger than 100 nm, which is still not within the nano range. Large amount of heat generated during machining and burnishing can cause the refined grains to grow significantly, and thus impeding the use of these two processes as effective *SPD* methods to produce nano/ultrafine grains. Calistes et al. [8] found nanocrystalline grains on the machined surface, and they purposefully used very mild cutting conditions, including a very small cutting speed (0.6 m/min) and a small undeformed chip thickness (100~200 μm), to ensure minimal temperature rise during *SPD*. Without an effective cooling strategy, the grain-refined layer becomes very thin and unstable due to the heat accumulated beneath the surface.

Cryogenic *SPD* processes, where liquid nitrogen is applied during processing, remarkably decreasse the temperature at the deformation zone, leading to nanocrystalline grain structures and a thicker grain-refined layer. Very few researchers have explored the potential of cryogenic *SPD* processes. Li et al. [9] cooled a copper rod to -173 deg. K using liquid nitrogen, and then used a surface mechanical grinding treatment (*SMGT*) to process the surface repeatedly up to six times to successfully produce a gradient nano-microstructured surface layer. The average grain size varied from about 22 nm in the top-most surface to sub-microns at about 200 μm deep, corresponding to a gradient change in hardness from 2.1 GPa near the surface to 1.1 GPa in the coarse-grained matrix. Nanostructures in copper were achieved from the machining experiments where the setup was immersed in liquid nitrogen [8].

In addition to nano/ultrafine grain structures, the application of liquid nitrogen can also introduce favorable residual stress distributions, which may further improve the functional performance of metallic materials. Compared with conventional oil-based cooling, Fredj and Sidhom [10] found that cryogenic cooling led to about 50% reduction of the tensile residual stress in the parallel direction, and in the perpendicular direction it was reduced to about zero from 200 MPa. They also show that the reduced tensile residual stresses generated by cryogenic grinding were reported to substantially improve the fatigue life of *AISI 304* steel, subjected to high-cycle fatigue loading. While numerous studies on cryogenic machining focus on tool-wear [11, 12], only very little has been reported on residual stresses developed due to cryogenic machining. Zurecki et al. [13] show that in cryogenic machining of *AISI 52100* steel the residual stress distribution was significantly improved. The application of liquid nitrogen during *SPD* processes has a great potential to produce a thick layer of nano/ultrafine grain structures, as well as compressive residual stresses simultaneously. This potential has not been adequately explored as yet, and this is the major focus of the current study of various materials reported in this paper.

2. EXPERIMENTAL WORK

2.1 Machining and Burnishing Setup

The experimental setup to conduct cryogenic processing is shown in Figure 1(a). A Mazak CNC Turning Center, equipped with an Air Products liquid nitrogen delivery system, is used for conducting machining experiments: both in orthogonal (Figure 1 (b)); and 3-D configurations, typically turning. Burnishing experiments were carried out using a custom-built burnishing tool, shown in Figure 1(c). Compared with cryogenic machining, this tool introduces more *SPD* into the workpiece, thus enabling modification of the subsurface microstructure at greater depths.

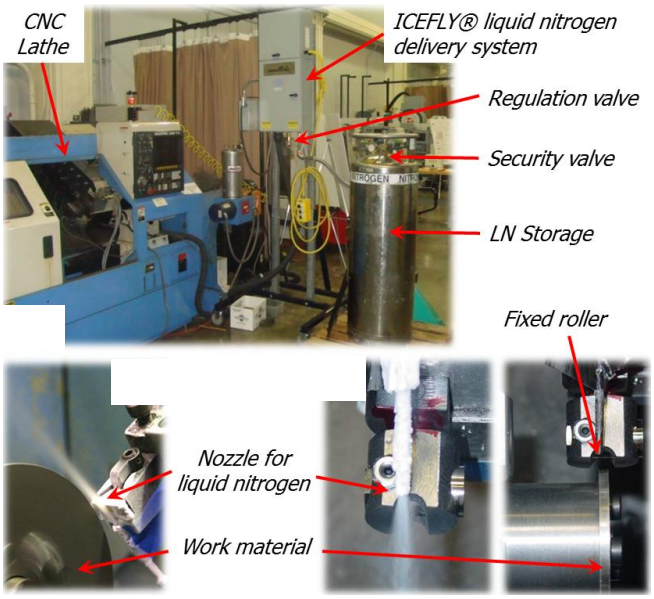

Fig. 1 (a) Mazak Quick Turn 10 Turning Center equipped with a liquid nitrogen delivery system; (b) Application of liquid nitrogen during cryogenic orthogonal machining of *AZ31B Mg* alloy; (c) experimental setup for cryogenic burnishing of *Co-Cr-Mo* alloy

2.2 Material Characterization

Metallurgical specimens were cut from the processed discs. After mounting, grinding, and polishing, the specimens were chemically etched by using corresponding etchants to reveal their microstructures. Microhardness and microstructure in the surface region were also measured before and after the processing. Microindentation tests were conducted by using a Vickers indenter on a CSM Micro-Combi Tester. Microstructural analysis was conducted using optical and scanning electron microscopes (*SEM*). Surface roughness of each ma-

chined surface was measured by a Zygo® optical interferometry-based surface profilometer. Finally, the crystal structures on the surfaces were analyzed using a X-ray equipment, Bruker AXS D8 Discover.

3. RESULTS AND DISCUSSION

3.1 Cryogenic Machining of *AZ31Mg* Alloys

One of the research issues in cryogenic machining is related to the nozzle position and how to apply liquid nitrogen to achieve optimal surface and subsurface integrity, in terms of grain refinement and residual stresses.

The potential of using cryogenic machining to control the microstructure on the surface and subsurface layers of *AZ31 Mg* alloy has been recently shown [14]. Cooling method and the edge radius of the cutting tool were found to have a significant influence on the microstructure resulting from machining as shown in Figure 2. In particular, Figure 2 (d) shows that in the affected layers grain structures were not discernible with both optical and *SEM* pictures. Under the same cutting conditions, dry machining did not produce any such significantly-affected layer (Figure 2 (b)). The layer thickness increased with tool edge radius. No differences in the chemical composition of this layer, compared with the bulk material, were found from the analysis of energy dispersive spectroscopy (*EDS*).

Fig. 2 Microstructure of *AZ31 Mg* alloy under optical microscope: (a) Before machining, and after (b) Dry machining, cutting edge radius = 30 µm, (c) Cryogenic machining, cutting edge radius = 30 µm, (d) Cryogenic machining, cutting edge radius = 70 µm [14]

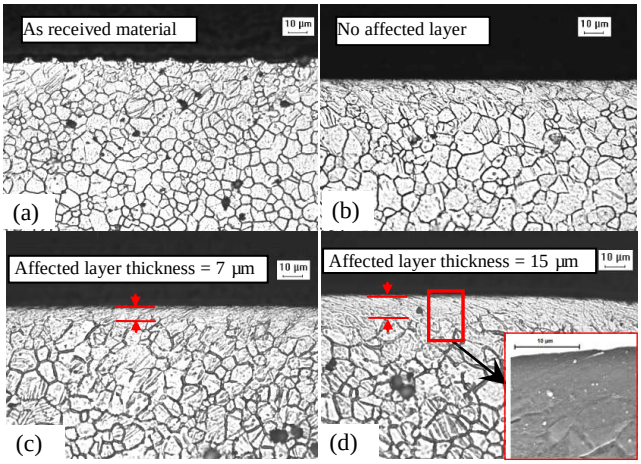

The grain size in the affected layer was measured using tapping mode atomic force microscopy (*AFM*). As shown in Figure 3, nanocrystalline grains of about 31 nm in size were formed on the machined surface. After cryogenic machining, the hardness in the affected layer increased to about 95 HV from 55 HV in the bulk material. These results highlight the need for a systematic investigation of cutting conditions on surface integrity changes in cryogenic machining. It is hoped that using relevant modeling techniques, the desired microstructure and residual stresses can be produced by proper machining conditions.

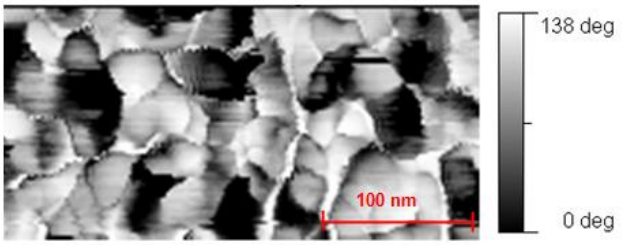

Fig. 3 Tapping-mode AFM picture of the surface from cryogenic machining of *AZ31 Mg* alloy with 70 µm edge radiused tool [14]

Recent findings at the University of Kentucky [15] demonstrate that the cryogenic machining could also improve the corrosion resistance of the *AZ31 Mg* alloy. It offers a great opportunity to produce/fabricate a grain-refined layer using cryogenic machining with improved corrosion resistance.

3.2 Cryogenic Burnishing of *AZ31 Mg* Alloy

Several points in transition in the affected layer from cryogenic burnishing of *AZ31 Mg* alloy, are shown in Figure 4 (a) demonstrating the *DRX* phenomenon. There is a clear interface between the process-influenced zone and the bulk. The total thickness of the process-influenced layer is 3.40 ± 0.01 mm. In addition to grain size, a strong basal texture, which was found to increase the corrosion resistance [16], was produced on the burnished surface, as shown in Figure 4 (b).

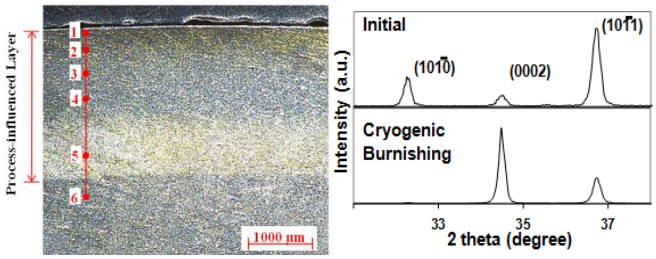

(a) (b)

Fig. 4 (a) Microstructure after cryogenic burnishing (×30 magnification) and (b) changes in crystallographic orientation after cryogenic burnishing [17]

The microstructures at different points are shown in Figure 5 at a ×5000 magnification. The image at Point 6 represents the initial microstructure and Point 1 is the microstructure near the surface after cryogenic burnishing. It is clear that significant grain refinement occurred near the surface. From Point 2 to Point 4, represent a transition zone, there is a clear trend with decreasing amount of ultra-fine grains. The grain structure within region below 15 µm is of great interest, and analysis of material properties in this layer is still ongoing.

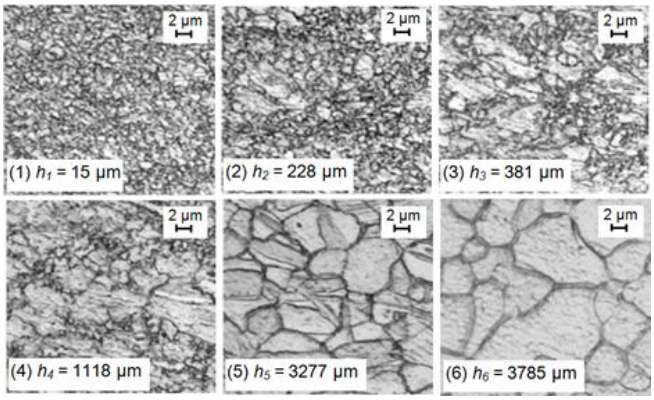

Fig. 5 Microstructures at different depths after cryogenic burnishing (×5000 magnification) [17]

Fatemi-Varzaneh et al. [18] investigated the effects of temperature, strain and strain-rates on *DRX* of *AZ31 Mg* alloy, and reported that the amount of dynamically recrystallized grains increased with strain in a sigmoid form. The strain induced by cryogenic burnishing should decrease from the surface to the bulk material where the material was not influenced by the process. This agrees with the literature that the amount of dynamically recrystallized grains will decrease when the strain is reduced.

3.3 Machining of *Co-Cr-Mo* Biomaterial

Our prior research on machining of *Co-Cr-Mo* alloys, which was primarily targeted at improved wear performance, shows that controlled machining processes could greatly improve wear resistance [19].

Pin-on-disc wear tests were conducted to evaluate the wear performance of machined pins. The influence of different machining conditions used in making the pin specimens such as cutting speed, depth of cut, feed and tool nose radius, on the wear rate of *Co-Cr-Mo* alloys was investigated. A genetic algorithm-based procedure was developed and used to determine the optimal cutting parameters for minimized wear/debris generation while satisfying the optimization constraints of surface roughness, surface microhardness and surface residual stress. Figure 6 shows a 2D contour plot of cutting speed vs. depth of cut. The yellow region represents the feasible region, while the red-cross locates the overall optimum point for minimized wear. All the contours with different colors and shapes correspond to different process output characteristics (wear, surface roughness, microhardness, hoop residual stress and radial residual stress). These plots help to select the right cutting parameters for achieving the most desired process characteristics [19].

3.4 Cryogenic Burnishing of *Co-Cr-Mo* Biomaterial

The cryogenic burnishing process has shown to improve the surface quality of hard materials such as *Co-Cr-Mo* alloy [20]. In comparison with the initial microstructure prior to burnishing, the microstructure of the surface regions after cryogenic burnishing is not discernible (Figure 7 (a) and (b)).

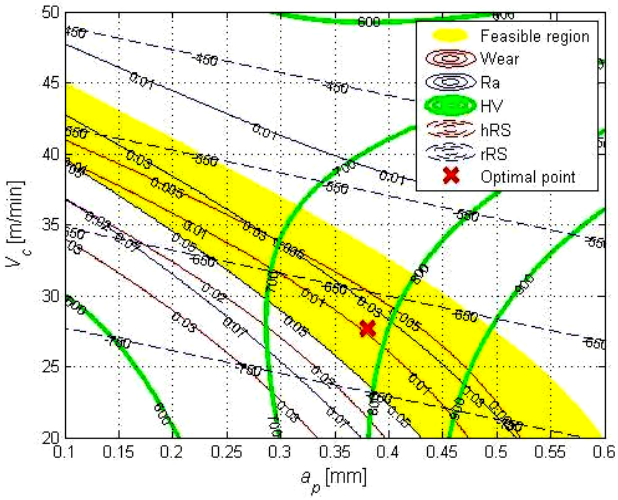

Fig. 6 2D Optimization contour plot of cutting speed vs. depth of cut for minimized wear of machined *Co-Cr-Mo* alloy [19]

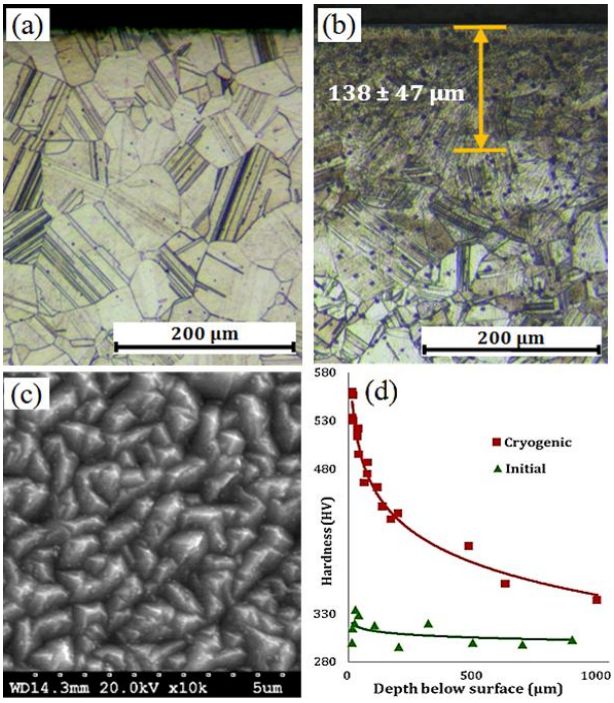

Fig. 7 Microstructures of *Co-Cr-Mo* samples: (a) initial microstructure, (b) after cryogenic burnishing; (c) SEM graph for near surface microstructure in (b); and (d) subsurface microhardness profiles [20]

This is due to significant grain refinement. The hardness of the surface layer after cryogenic burnishing was increased by about 90% (Figure 7 (d)). Typical microstructures near the topmost surface are shown in an *SEM* picture in Fig. 7(c). While the average grain size in the longitudinal axis is 80 μm for the initial material, the grain size in the topmost surface after cryogenic burnishing reduced to submicron level.

The smallest grain size achieved was 300 nm. Therefore, it is evident that thick surface layers with remarkable grain refinement occurred due to the *SPD*-induced (*DRX*) and the effective cryogenic cooling.

In addition to grain refinement, the crystal structure of the *Co-Cr-Mo* alloy is another critical factor which significantly influences its performance as joint implants. It has been reported that the wear behavior of *Co-Cr-Mo* alloys with higher amount of *hcp* structure was superior to the ones with less *hcp* or pure *fcc* structure [21]. As shown in Figure 8, the application of cryogenic cooling significantly increased the formation of *hcp* structure during burnishing [20], and this is due to the accelerated *fcc* to *hcp* transformation in cryogenically-induced rapid cooling rates [22].

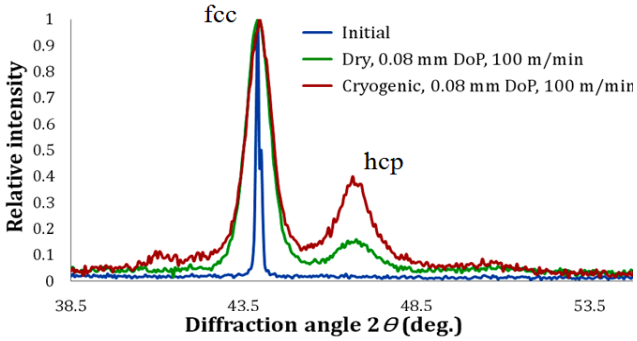

Fig. 8 *XRD* patterns on *Co-Cr-Mo* alloy [20]

3.5 Cryogenic Machining of *Inconel 718* Alloy

One of the major indicators of surface integrity of machined components is surface roughness, whose control may contribute to the enhanced hardness and improved subsurface microstructure leading to positive impact on fatigue life of machined components [23].

The measured results, shown in Figure 9, illustrate that cryogenic cooling produces better surface quality in comparison with dry machining. It is clearly shown in Figure 9 that the difference is attributed to the surface topology. Surface topology is considered as one of the surface integrity parameters. Particularly in turning process, the produced feed marks on the machined surface may lead to increased possibility of starting fatigue crack at the surface due to the irregularities. The surface topologies of machined surface show that feed marks are more visible on the dry machined sample; however, cryogenic machining produces a smoother surface with the reduced height of the feed mark, and consequently produces a better surface roughness.

According to Herbert et al. [24] different intensity and width of peak in *XRD* results represent different grain size. It is clearly seen in Figure 10, the width of peak broadened and intensity shortened with cryogenic machining which proves that grain refinement took place and smaller grains are generated on the surface and subsurface of machined components, thus leading to increased strength and durability of machined components.

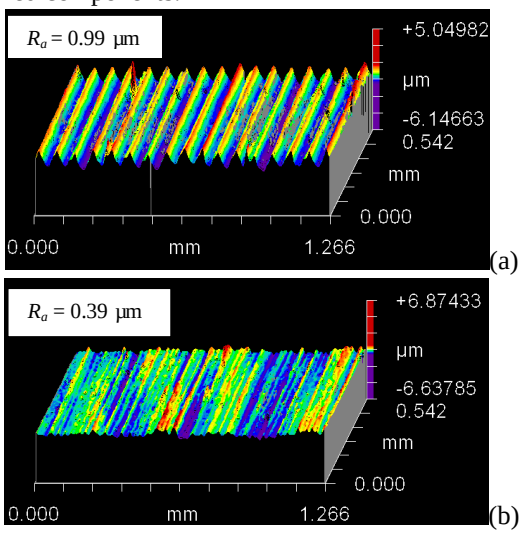

Fig. 9 Surface topology and roughness of machined *Inconel 718* samples from (a) dry, and (b) cryogenic machining (V = 60 m/min, f = 0.075 mm/rev, d = 0.77 mm, *CNMG120408*)

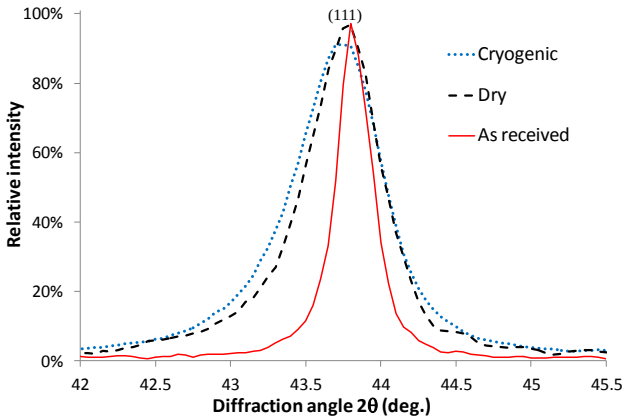

Fig. 10 *XRD* patterns of machined *Inconel 718* samples (V = 60 m/min, f = 0.075 mm/rev, d = 0.77 mm, *CNMG120408*)

The smaller grains obtained from cryogenic cooling conditions are resulting from the dynamic recrystallization (*DRX*), which is due to the severe plastic deformation process.

3.6 Cryogenic Machining of *NiTi* Shape Memory Alloy

Figure 11 shows the measured surface roughness results of $Ni_{49.9}Ti_{50.1}$ shape memory alloy (SMA) in turning operations under dry and cryogenic cooling conditions using CNMG 120404-MF1 890 tool inserts. As expected, in both machining conditions, at lower feed rate values, good surface generated, and the surface roughness is always lower with cryogenic machining than in dry machining for all selected feed rates. Also, it is noted that the cryogenic machining provides a lower rate of increase in surface roughness with feed rate, in comparison with dry machining, and this is an advantage

in some applications with higher feed rates being used in the final finish operation. Thus, no additional processes such as grinding would be required for *NiTi* SMA components.

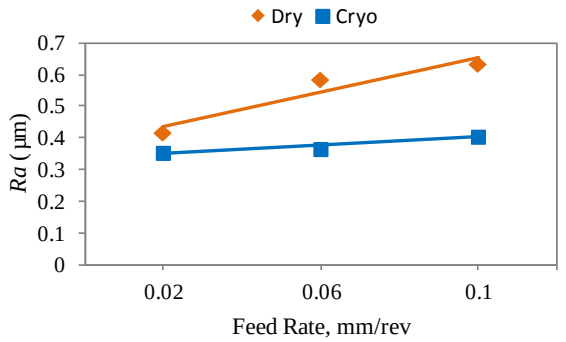

Fig. 11 Surface roughness (R_a) comparison in machined *NiTi* SMAs (V = 80 m/min, f = 0.02 m/rev; d = 0.65 mm; *CNMG 120404-MF1 890*) [23]

The hardness of material is one of the important mechanical properties and is among the major surface integrity characteristics of machined components. The material hardness is directly related to the yield strength of the material. Micro-hardness of cryogenically machined sample, dry machined sample and virgin material have been compared in the machined surface layer within the first 200 µm depth from the machined surface – see Figure 12.

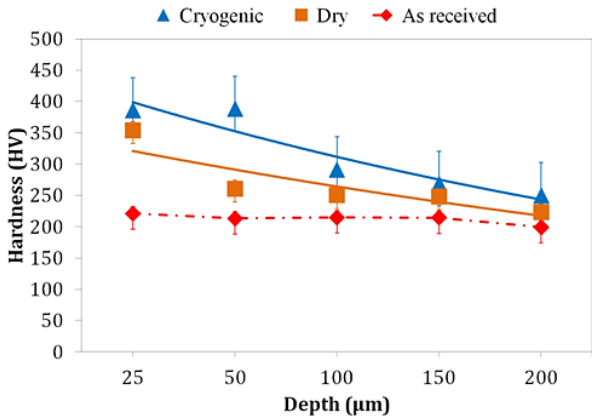

Fig. 12 Comparison of hardness depth profiles in the subsurface of *NiTi* SMAs (V = 80 m/min, f = 0.02 m/rev; d = 0.65 mm; *CNMG 120404-MF1 890*) [23]

Both machining methods result in increased microhardness in the subsurface of machined samples. Obtained results also indicate that although hardness values reduce with increase in depth, cryogenic machining consistently demonstrates the higher strain-hardening effect of *NiTi* SMAs in the subsurface region. This point is important for material`s durability because it is well established that components under operating/service conditions fail largely due to fatigue and the failure generally starts at the surface. Increased hardness promotes improved durability, wear and fatigue resistance of machined components, and thus improved product sustainability.

3.7 Cryogenic Machining of *AA7075-T651* Alloy

Recent experimental work in dry and cryogenic turning of *AA7075–T651* alloy is aimed at achieving environmental benefits and improved surface integrity and fatigue life of the machined products [25]. Figure 13 shows the effect of the dynamic recrystallization occurring during the machining process.

More precisely, all examined samples present a refinement of the mean grain diameter from the bulk to the surface. The results show a profound surface grain refinement in the cryogenically machined samples, even though grain recrystallization takes place in all the performed tests.

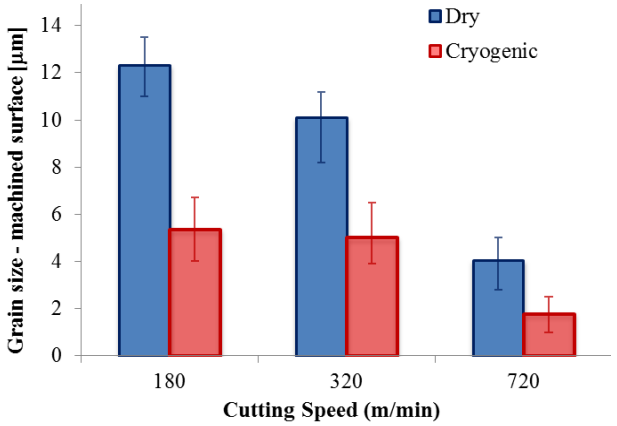

Fig. 13 Grain size refinement at varying cooling conditions and cutting speeds [25]

The micro-hardness, Vickers $HV_{0.05}$, of each sample was also measured in order to verify and correlate with the microstructural changes in the machined samples. The results shown in Figures 14 show that the hardness on the machined surface is higher in all cases tested. In particular, the cryogenic machining generates consistently higher hardness on the machined surface and within the subsurface layer than what was generated from dry machining.

Also, the fatigue life of machined *AA7075–T651* alloy depends on the surface grain size and the initiation portion of its life, and this can be predicted by using a microstructure-based model established by Chan [26] as reported in Eq. (1):

$$(\Delta\sigma - 2Mk)N_i^{\alpha} = \left[\frac{8M^2\mu^2}{\lambda\pi(1-\nu)}\right]^{\frac{1}{2}}\left(\frac{h}{d}\right)\left(\frac{c}{d}\right)^{\frac{1}{2}} \qquad (1)$$

Equation (1) has been adapted in [25] in order to estimate the fatigue life of finished parts/components and to compare the effect of the turning processes on fatigue life via the surface microstructure.

The overall results [25] show that cryogenic cooling has the potential to improve the machined surface and sub-surface

characteristics and the related environmental and economic performance (Figure 15).

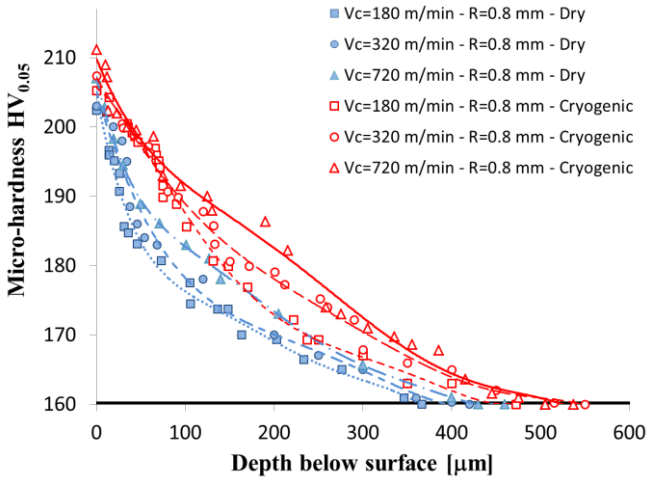

Fig. 14 Measured micro-hardness under dry and cryogenic cooling conditions at varying cutting speeds [25]

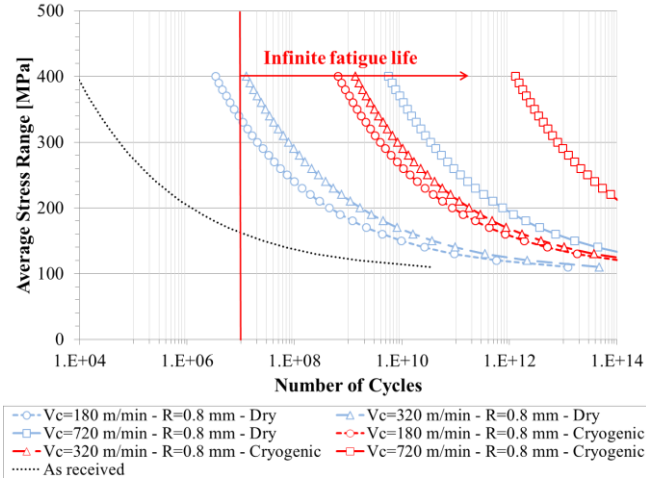

Fig. 15 Calculated fatigue life for the measured superficial grain size at varying cutting speeds and cooling methods [25]

3.8 Cryogenic Machining of *AISI 52100* Alloy

Recent experimental work [27] has established the effects of cryogenic cooling on surface integrity in orthogonal machining of hardened *AISI 52100* steel. Figure 16 shows the experimental white layer thickness produced at varying cutting speeds under dry and cryogenic cooling conditions.

The white layer produced on the machined surface (also known as the severe plastically deformed layer, SPD) ranges from less than 1 µm in cryogenic conditions to more than 7 µm in dry machining. Furthermore, the white layer slightly increases with the increasing cutting speed. Amazingly, the white layer thickness from cryogenic cooling is much smaller than the white layer thickness from dry machining. This observation is in agreement with the experimental results by Zurecki et al [13]. Figure 17 shows the phase analysis obtained from the *XRD* technique on both samples (machined under dry and cryogenic cooling conditions) that produce white layers, and its comparisons with unmachined sample with no presence of any white layer.

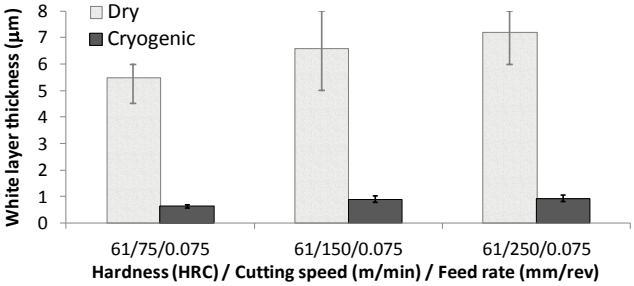

Fig. 16 White layer thickness at varying cutting speeds in dry and cryogenic machining (Workpiece hardness = 61 HRC and Feed rate = 0.075 mm/rev) [27]

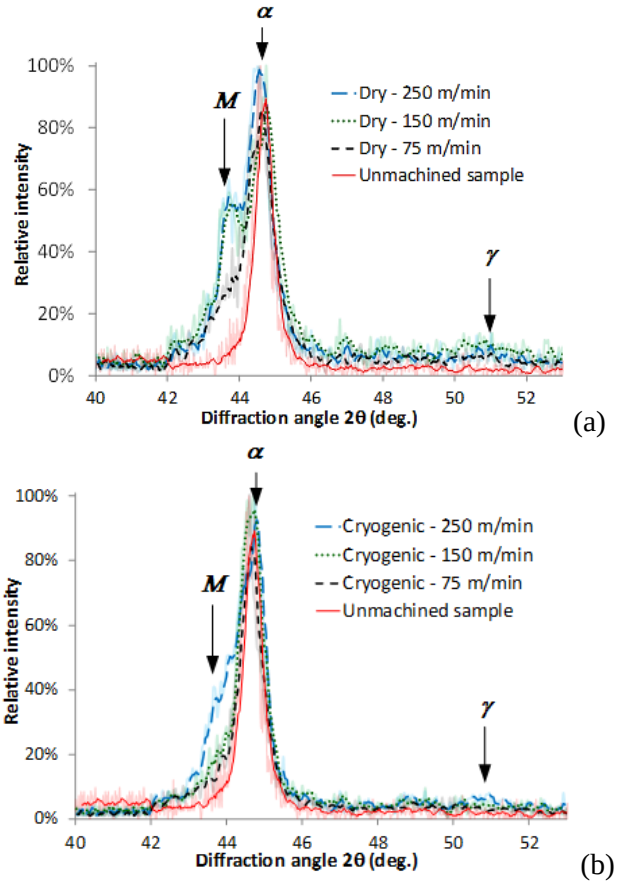

Fig. 17 X-ray phase analysis on specimens machined in (a) dry conditions and (b) cryogenic conditions and comparisons with unmachined samples (Workpiece hardness = 61 HRC and Feed rate = 0.075 mm/rev, and Chamfered tool) (α = ferrite-α; γ = austenite; *M* = martensite) [27]

In particular, the X-ray phase analysis on the unmachined surface shows only one peak at 44.67 °which corresponds to ferrite-α at (110) Miller's indices. In contrast, when samples machined under dry condition were investigated, the X-ray

phase analysis shows several peaks (Figure 17 (a)). Once again, one peak is located at 44.67 °, which corresponds to ferrite-α. Also, two additional peaks are found at 43.74 ° and 50.67 °. Specifically, the peak at 43.74 ° in Figure 17 (a) corresponds to martensite (102), while the peak at 50.67 ° corresponds to retained austenite at (200) Miller's indices.

In contrast, the X-ray phase analysis conducted on sample machined under cryogenic cooling (Figure 17 (b)) still shows the peaks referred to as ferrite-α, whereas the peak related to martensite shows a significantly lower relative intensity (especially at 75 and 150 m/min cutting speeds). The peaks referred to the austenite are slightly higher (at 250 m/min) or similar (at 75 and 150 m/min) to those detected on the unmachined samples (Figure 17 (b)). As the white layer is generally formed as a result of rapid heating and quenching (formation on untempered martensitic structure), this experimental evidence shows that this layer is drastically reduced when hard machining is carried out with cryogenic cooling, i.e., less microstructural transformation due to the cooling method, which keeps the temperature below the estimated austenite-start temperature during machining of hardened steels.

3.9 Residual stresses and corrosion performance of cryogenically machined *AZ31B Mg* alloy

The residual stresses measured before and after cryogenic machining of *AZ31 Mg* alloy using a tool with 70 µm edge radius are shown in Figure 18 [28].

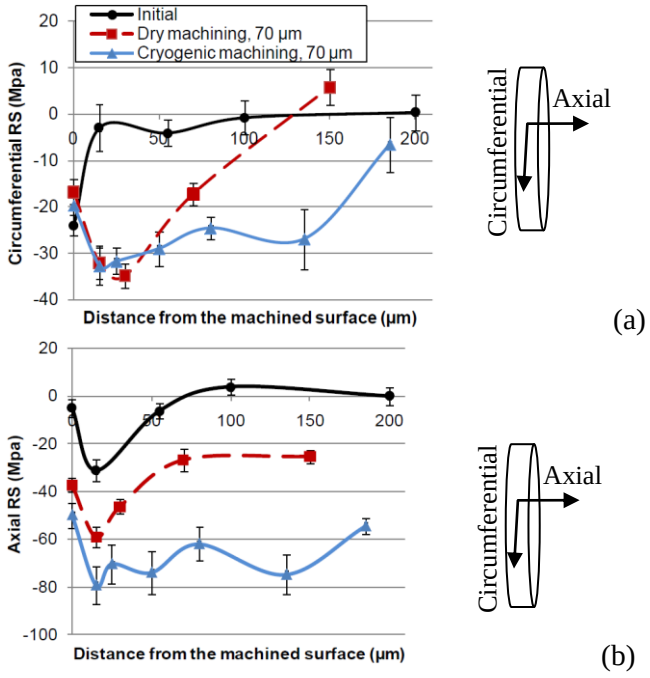

Fig. 18 Comparison of residual stresses before and after cryogenic machining of *AZ31 Mg* alloy using a tool with 70 µm edge radius (b) circumferential and (c) axial direction [28]

The residual stresses before machining (initial residual stress shown in Figure 18) in both directions were close to zero when the distance from the surface reached about 100 µm. After cryogenic machining, compressive residual stresses are found in both circumferential and axial directions. The residual stresses in the axial direction are much more compressive than in the circumferential direction. The maximum compressive residual stresses are located below the machined surface and are -33 MPa in the circumferential direction and -79 MPa in the axial direction, which is very close to the compressive yield stress of *AZ31 Mg* alloy (110 MPa). The thickness of the compressive layer is greater than 200 µm. A greater area limited by the residual stresses profiles and the x-axis can be found after cryogenic machining when compared with before machining. Therefore, a significant improvement in the functional performance of the machined *AZ31 Mg* discs with respect to corrosion properties is expected after cryogenic machining

The corrosion resistance of *AZ31 Mg* alloy after cryogenic machining was evaluated using a hydrogen evolution method. The preliminary results shown in Figure 19 demonstrate that cryogenic machining could improve the corrosion resistance of the *AZ31 Mg* alloy, which may be due to grain refinement and compressive residual stresses

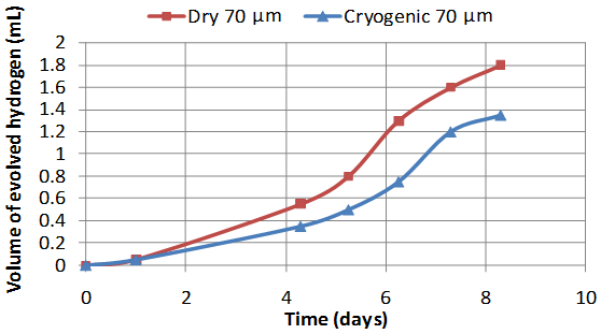

Fig. 19 Hydrogen evolution during in vitro corrosion test under different machining conditions [29].

4. FUNCTIONAL PERFORMANCE OF CRYOGNICALLY PROCESSED COMPONENTS

Cryogenically processed components in general acquire significant grain refinement, often with nano-grains, in the SPD layer adjacent to the processed surfaces. The mechanical properties of this layer are significantly altered: with increased hardness, and hence the greater wear resistance; reduced corrosion rate with improved corrosion resistance; and often with compressive residual stresses that are larger in magnitude and at greater depth. The latter leads to improved fatigue life of cryogenically processed components. This property improvement, with wear and corrosion resistance and fatigue life, is indeed a product sustainability benefit contributing to the durability and improved function-

al performance of cryogenically processed components during their service life [30].

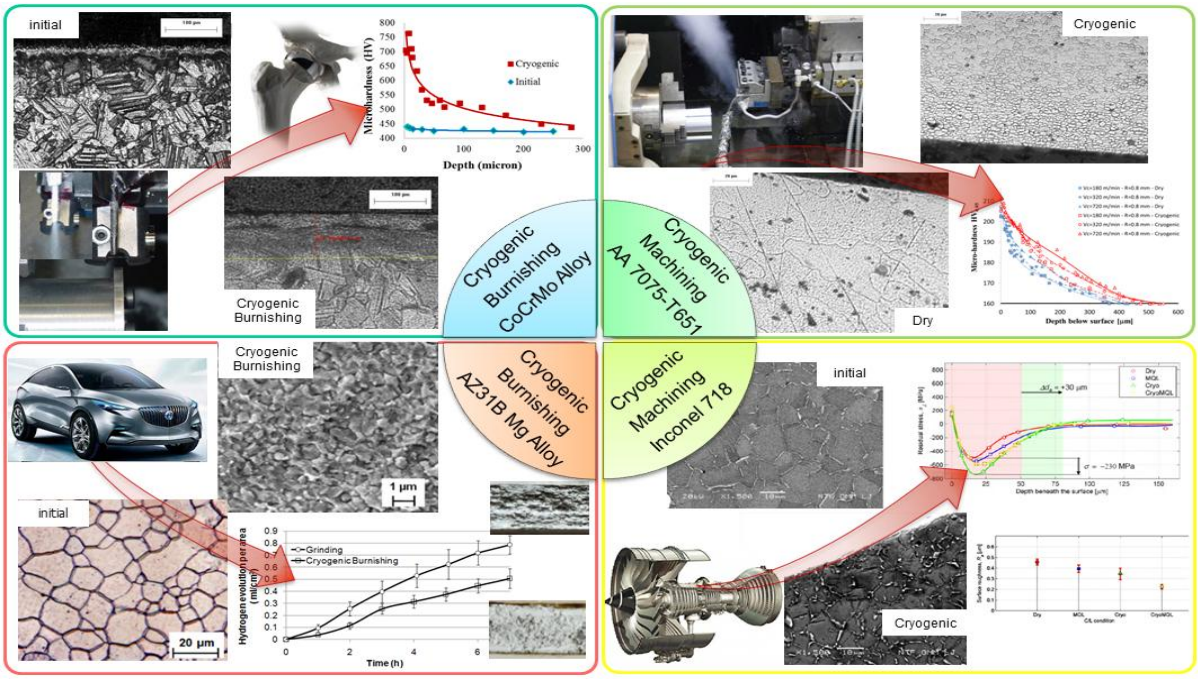

Fig. 20 Property improvement and potential applications of cryogenic processing.

Figure 20 illustrates a summary of improved functionality of components produced from cryogenic processing. Figure 20 (a) shows the grain refinement and surface and sub-surface hardening generated from the cryogenic burnishing of Co-Cr-Mo biomaterial which results in reduced debris generation and improved fatigue life for applications in biomedical hip and knee implants. Figure 20 (b) shows the major benefit of producing grain refinement and the associated surface hardening from cryogenic machining of *AA 7075-T651* aerospace alloy Figure 20 (c) shows the significant grain refinement and reduced corrosion rate in *AZ31B Mg* alloys with potential automotive applications, while Figure 20 (d) shows the generation of compressive residual stresses and improved surface roughness from machining of Inconel 718 from cryogenic machining and their potential aerospace applications.

5. SUMMARY AND CONCLUSIONS

This paper has shown that cryogenic machining and burnishing processes can produce *SPD* with improved surface integrity in the surface region of different metallic materials resulting in improved product performance.

AZ31 Mg alloy was subjected to both cryogenic machining and burnishing processes. Significant surface grain refinement from 12 µm down to 500 nm from cryogenic burnishing and 45 nm after cryogenic machining was achieved. Cryogenic burnishing remarkably change the microstructure up to about 3.4 mm deep into the surface, while the influence of cryogenic machining is limited to the top 20 µm. Corrosion test shows that after cryogenic machining and burnishing the corrosion resistance of the processed *AZ31 Mg* alloy was enhanced. Results from machining of *Co-Cr Mo* alloy show that the optimal combination of machining parameters significantly reduced the wear generation (50%) in metal-on-metal hip implants due to compressive residual stresses. It eliminates the need for costly and time-consuming post-manufacturing treatments, such as the use of special coatings or additional heat treatment. Cryogenic burnishing of *Co-Cr-Mo* alloy resulted in significant grain refinement in the surface region through burnishing-induced *SPD*. Microhardness in the *SPD* layer was increased up to 90% relative to the bulk value.

Experimental work of machining *Inconel 718* alloys under dry and cryogenic cooling conditions shows that cryogenic cooling substantially improves the surface quality of machined parts. By effectively removing the generated heat from the newly machined surface, it prevents growing refined grains as a result of *DRX*. It is well established that smaller grains on surface and subsurface improve mechanical properties of the machined products.

Experimental work shows that cryogenic machining significantly helps to improve the surface and sub-surface quality of the machined *Ni-Ti* SMAs compared with dry machining conditions. Thermo-mechanical properties of *Ni-Ti* SMAs have been improved with cryogenic machining process through significantly increased subsurface microhardness.

Results from machining of *AA 7075-T651* alloy shows that cryogenic coolant significantly influences the grain refine-

ment of the final product, which results in a better surface hardness and fatigue life performance.

Results from machining of *AISI 52100* steel suggest that the use of cryogenic coolant significantly reduces the white layer thickness. Also, the experimental results prove that the microstructural phase changes are heavily influenced by the use of the cryogenic cooling and, in some cases, leading to the total removal of martensite.

This extensive study reveals a good and unique opportunity to use cryogenic machining and burnishing, which are simple and cost-effective manufacturing processes, to remarkably enhance functional performance of metallic materials, such as corrosion/wear/fatigue resistance by inducing ultrafine/nano microstructures in the surfaces layer.

Acknowledgments

We sincerely thank Air Products and Chemicals for providing the equipment for cryogenic processing. Also, special thanks are due to ISM technical staff, Charles Arvin for his valuable help throughout the experimental work.

References

1. S. Swaminathan, M. R. Shankar, S. Lee, J. Hwang, A. H. King, R. F. Kezar, B. C. Rao, T. L. Brown, S. Chandrasekar, W. D. Compton and K. P. Trumble, Materials Science and Engineering: A, 410, 358 **(2005).**
2. C. Saldana, S. Swaminathan, T. L. Brown, W. Moscoso, J. B. Mann, W. D. Compton and S. Chandrasekar, J. Mfg. Sci. and Engg., 132. 030908-1-12 **(2010)**.
3. A. Ramesh, S. N. Melkote, L. F. Allard, L. Riester and T. R. Watkins, Materials Science and Engineering: A, 390, 88 **(2005).**
4. H. Sasahara, Int. J. Machine Tools and Manufacture, 45, 131 **(2005)**.
5. P. Zhang and J. Lindemann, Scripta Materialia, 52, 1011 **(2005).**
6. I. Nikitin, I. Altenberger, H. J. Maier and B. Scholtes, Materials Science and Engineering: A, 403, 318 **(2005)**.
7. G. H. Majzoobia, K. Azadikhahb and J. Nematia, Materials Science and Engineering, 516, 235 **(2009).**
8. R. Calistes, S. Swaminathan, T. G. Murthy, C. Huang, C. Saldana, M. R. Shankar and S. Chandrasekar, Scripta Materialia, 60, 17 **(2009).**
9. W. L. Li, N. R. Tao and K. Lu, Scripta Materialia, 59, 546 **(2008)**.
10. B. Fredj and H. Sidhom, Cryogenics, 46, 439 **(2006).**
11. S. Hong, J. Mfg. Sci. and Engg., 123, 331 **(2001).**
12. R. Ghosh, Trans. of NAMRI/SME, 33, 161 **(2005).**
13. Z. Zurecki, R. Ghosh and J. H. Frey, Investigation of white layers formed in conventional and cryogenic hard turning of steels, Proc. of IMECE'03, **(2003)** November 16-21, Washington, D.C.
14. Z. Pu, J. C. Outeiro, A. C. Batista, O. W. Dillon Jr, D. A. Puleo and I. S. Jawahir, Int. J. Machine Tools and Manufacture, 56, 27 **(2012)**.
15. Z. Pu, G. L. Song, S. Yang, J. C. Outeiro, O. W. Dillon Jr, D. A. Puleo and I. S. Jawahir, Corrosion Science 57, 192 **(2012)**.
16. G. Song, R. Mishra, Z. Xu, Electrochem. Commun., 12, 1009 **(2010).**
17. Z. Pu, S. Yang, G. L. Song, O. W. Dillon Jr, D. A. Puleo and I. S. Jawahir, Scripta Materialia 65(6), 520 **(2011).**
18. S. M. Fatemi-Varzaneh, A. Zarei-Hanzaki, H. Beladi, Materials Science and Engineering A, 456, 52 **(2007).**
19. A. Deshpande, S. Yang, D. Puleo, D. Pienkowski, O.W. Dillon Jr., J.C. Outeiro, I.S. Jawahir, Minimized wear and debris generation through optimized machining of *Co-Cr-Mo* alloys for use in metal-on-metal hip implants. In: 7th ASME Int. Mfg. Science and Engineering Conf. (MSEC2012). Notre Dame, IN, **(2012)** June 4-8.
20. S. Yang, Cryogenic Burnishing of Co-Cr-Mo alloy for enhanced surface integrity and improved wear performance, Ph.D. Dissertation, University of Kentucky **(2012).**
21. A. J. Saldivar-Garcia and H. F. Lopez, J. Biomedical Materials Research Part A, 74A(2), 269 **(2005).**
22. A. E. Ray, S. R. Smith and I. D. Scofield, J. Phase Equilibria, 12(6) **(1991).**
23. Y. Kaynak, H.E. Karaca and I.S. Jawahir, Cryogenic machining of *NiTi* Shape Memory Alloys. In: 6th Int. Conf. on Design and Production of Machines and Dies/Molds, Ankara, Turkey, **(2011)** June 23-26.
24. C. Herbert, D. Axinte, M. Hardy and P.D. Brown, Machining Science and Technology 16(1), 40 **(2012)**
25. G. Rotella, T. Lu, L. Settineri, O. W. Dillon and I. S. Jawahir, Dry and Cryogenic Machining: Comparison from the Sustainability Perspective. In: 9th Global Conf. on Sustainable Manufacturing, Saint Petersburg, **(2011)** September 28-30.
26. K. S. Chan, Metallurgical and Materials Transactions A, 34, 43 **(2003).**
27. D. Umbrello, S. Caruso, Z. Pu, J. C. Outeiro, A. D. Jayal, O. W. Dillon and I. S. Jawahir, Procedia Engineering, 19, 371 **(2011)**.
28. Z. Pu, J. C. Outeiro, A. C. Batista, O. W. Dillon, D. A. Puleo and I. S. Jawahir, Procedia Engineering, 19, 282 **(2011)**.
29. Z. Pu, D. A. Puleo, O. W. Dillon and I. S. Jawahir, Controlling the biodegradation rate of magnesium-based implants through surface nanocrystallization induced by cryogenic machining, In: Proceeding of Magnesium Technology 2010, TMS Annual Meeting. Seattle, WA **(2010)** February 14-18.

30. I.S. Jawahir, E. Brinksmeier, R. M'Saoubi, D.K. Aspinwall, J.C. Outeiro, D. Meyer, D. Umbrello and A.D. Jayal, Annals of the CIRP, 60(2), 603 **(2011).**